Solution of the Boundary Layer Equations for a Rotating Cone in Supersonic Flow

Research Project

Author: Shahaf Haiman
Advisor: Dr. Michael Karp

Flow Physics Lab, Faculty of Aerospace Engineering
Technion - Israel Institute of Technology

October 2024

Abstract

This research project deals with the solution of the flow field in the boundary layer for a rotating cone in supersonic flow. The study begins by outlining the physical problem, emphasizing the complexities arising from the interaction between rotation and supersonic flow. The mathematical framework is established through the derivation and transformation of the boundary layer equations from the Navier-Stokes equations, leveraging the Stewartson-Illingworth transformation to facilitate similarity solutions. A critical assumption regarding the decoupling of the azimuthal momentum equation enables the application of various numerical methods for solving the resulting ordinary differential equations. This work is related to numerous applications in the industry, such as the flow over engine inlet cones (e.g. the SR-71 "Blackbird" inlet, Fig. (1)) and the flow fields around projectiles.

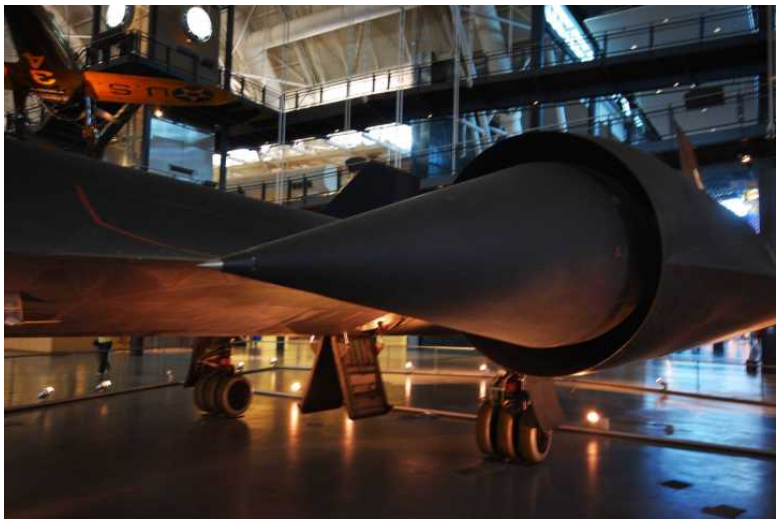

Figure 1: Engine inlet cone of the Lockheed SR-71 "Blackbird"

Contents

List of Figures

Nomenclature

Notation

$\bar{\bar{\tau}}$	Shear stress tensor
$\bar{\bar{I}}$	Identity tensor
$\bar{C}_1$	Constant (arbitrary)
δ	Boundary layer thickness
γ	Heat capacities ratio
κ	Heat conductivity
$\mathcal{H}$	Function which is constant on streamlines
μ	Dynamic viscosity
Ω	Cone's angular velocity
ρ	Density
σ	Viscosity's power law coefficient
θ_c	Cone's half-angle
θ_s	Shock angle
ε	Total specific energy
$\vec{\nabla}$	Nabla operator
$\vec{X}$	State vector, see Eq. (29)
$\vec{u}$	Velocity vector
ξ, η	Transformed variables, see Eq. (19)
a	Speed of sound
C_p, C_v	Heat capacities at constant pressure and volume, respectively
e	Internal specific energy
F, Θ, G	Similarity functions, see Eq. (20)
h	Flight altitude
L	Streamwise length scale, cone's length
M	Mach number
p	Pressure
Pr	Prandtl number
R	Gas constant
Re	Reynolds number
T	Temperature
t	Time
T_0	Stagnation temperature
u, v, w	Velocity vector components in x, y, ϕ directions, respectively
U_∞	Flight velocity
V, W	Dimensional scales for v, w velocity components
x, y, ϕ	Coordinate system – parallel, normal to the body and azimuthal, respectively

Embellishments

$(\cdot)'$	Derivative with respect to η
$(\cdot)^T$	Transpose
$(\cdot)_\infty$	Freestream / flight conditions
$(\cdot)_e$	Boundary layer edge conditions
$(\cdot)_w$	Wall conditions
$\bar{\bar{(\cdot)}}$	Tensor quantity
$\hat{(\cdot)}$	Unit vector, direction
$\tilde{(\cdot)}$	Dimensionless quantity
$\vec{(\cdot)}$	Vector quantity

Abbreviations

AOA	Angle of attack
BC	Boundary condition
BL	Boundary layer
IVP	Initial-value problem
ODE	Ordinary differential equation
PDE	Partial differential equation
TM	Taylor-Maccoll

1 Introduction

The study of supersonic flows around axisymmetric bodies began with the work of Taylor & Maccoll (1933), where they solved for the flow field around a supersonic cone. In addition, the solution for flows around blunt bodies was found, where it was discovered that a bow shock creates entropy gradients and vorticity, as stated by Crocco's Theorem (Crocco, 1937).

Moreover, in the field of boundary layers, solutions for various problems have been established. Perhaps the most known one is the self-similar solution for the boundary layer of a steady incompressible flow on a semi-infinite flat plate, i.e. the Blasius boundary layer (Blasius, 1908). A generalization of the Blasius solution for a wedge (inclined flat plate) is the Falkner–Skan boundary layer (Falkner & Skan, 1931). Both Blasius and Falkner-Skan solutions have a compressible generalization, in which the density also varies in the flow field (e.g. Cohen & Reshotko, 1956).

The boundary layers on rotating bodies of revolution, which are a combination of the two presented fields (boundary layers and bodies of revolution), were also investigated. Illingworth (1953) studied the boundary layer equations on rotating bodies of revolution in compressible flow using the Mangler transformation (Mangler, 1948). The equations were solved for the case of a rotating cone in supersonic flow, using series expansion methods. A summary of axisymmetric and three-dimensional boundary layers is provided in the seminal book of Schlichting & Gersten (2017). This summary includes several works, such as similarity solutions for non-rotating axisymmetric boundary layers (Sedney, 1957; Pokrovskii *et al.*, 1984) and a solution of the boundary layer for a rotating cone at non-zero AOA in supersonic flow (Geis *et al.*, 1955).

In this study, a combination of both fields is also considered. The main goal is to find the solution for the boundary layer of a supersonic flow around a rotating cone, using similarity methods.

2 Physical Problem

Consider the steady flow over a cone-shaped body in Fig. (2). The flow is supersonic (i.e. $M_\infty > 1$), and therefore a conical oblique shock is formed around the cone. The shock angle θ_s can be determined by the cone half-angle θ_c and freestream mach number M_∞, as will be explained afterwards. In addition, the cone is rotating around its own axis, in an angular velocity Ω, and its surface temperature is T_w.

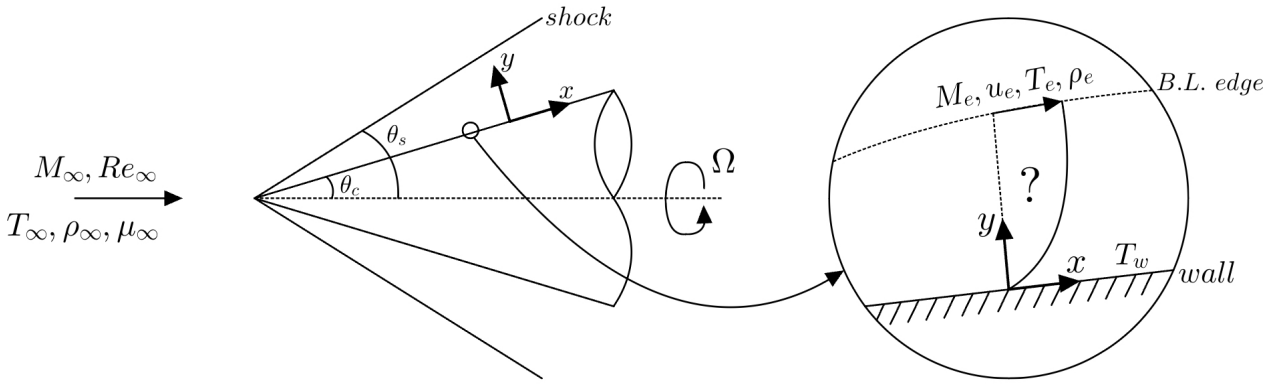

Figure 2: Schematic sketch of a cone-shaped body in supersonic flow and a boundary-layer zoom-in

The inviscid flow around a non-rotating cone was derived by Taylor and Maccoll (TM) (Taylor & Maccoll, 1933). Our focus is on solving the flow field in the boundary layer (BL) around the cone,

where the viscosity is dominant. Assuming that the BL is thin, the TM solution can be used as the BL edge conditions. Another assumption is that the azimuthal velocity is decaying throughout the BL to a vanishing edge value. Our analysis is aimed at finding the streamwise velocity profile, $u(y)$, illustrated in Fig. (2), as well as the temperature profile, $T(y)$, and azimuthal velocity profile, $w(y)$, inside the BL.

3 Mathematical Method

3.1 Governing Equations

The equations describing compressible, viscous flow are as following,

Continuity:

$$\frac{\partial \rho}{\partial t} + \vec{\nabla} \cdot (\rho \vec{u}) = 0, \tag{1}$$

Momentum:

$$\frac{\partial}{\partial t}(\rho \vec{u}) + \vec{\nabla} \cdot (\rho \vec{u}\vec{u}) + \vec{\nabla} p = \vec{\nabla} \cdot \bar{\bar{\tau}}, \tag{2}$$

Energy:

$$\frac{\partial}{\partial t}(\rho \varepsilon) + \vec{\nabla} \cdot (\rho \vec{u} \varepsilon) = -\vec{\nabla} \cdot (p \vec{u}) + \vec{\nabla} \cdot \left(\kappa \vec{\nabla} T\right) + \vec{\nabla} \cdot (\bar{\bar{\tau}} \cdot \vec{u}), \tag{3}$$

where $\varepsilon = e + \frac{|\vec{u}|^2}{2}$ is the total specific energy. These are supplemented by the ideal gas equation

$$p = \rho R T, \tag{4}$$

where $R = const.$ is the gas constant.

The following assumptions about the flow are applied:

1. Steady flow: $\frac{\partial}{\partial t} = 0$
2. Axisymmetric flow: $\frac{\partial}{\partial \phi} = 0$
3. Newtonian fluid: $\bar{\bar{\tau}} = \mu \left(\vec{\nabla}\vec{u} + \left(\vec{\nabla}\vec{u}\right)^T - \frac{2}{3}\left(\vec{\nabla} \cdot \vec{u}\right) \bar{\bar{I}} \right)$
4. Calorically perfect gas: $e = C_v T$, where $C_v = const.$
5. Constant Prandtl number: $\kappa = \frac{C_p \mu}{Pr}$, where $C_p, Pr = const.$
6. Power law for viscosity: $\mu = \mu_e \left(\frac{T}{T_e}\right)^\sigma$, where $\sigma = const.$

Let us rewrite the governing equations using the chosen coordinate system, as shown in Fig. (3). Let p be a scalar and $\vec{u} = (u, v, w)$ be a vector, the differential operators in these coordinates are:

$$\begin{aligned}
\vec{\nabla} p &= \frac{\partial p}{\partial x}\hat{x} + \frac{\partial p}{\partial y}\hat{y} + \frac{1}{x\sin\theta_c + y\cos\theta_c}\frac{\partial p}{\partial \phi}\hat{\phi}, \\
\vec{\nabla} \cdot \vec{u} &= \frac{\partial u}{\partial x} + \frac{\partial v}{\partial y} + \frac{u\sin\theta_c + v\cos\theta_c}{x\sin\theta_c + y\cos\theta_c} + \frac{1}{x\sin\theta_c + y\cos\theta_c}\frac{\partial w}{\partial \phi}, \\
\vec{u} \cdot \vec{\nabla} &= u\frac{\partial}{\partial x} + v\frac{\partial}{\partial y} + \frac{w}{x\sin\theta_c + y\cos\theta_c}\frac{\partial}{\partial \phi}, \\
\nabla^2 p &= \frac{\partial^2 p}{\partial x^2} + \frac{\partial^2 p}{\partial y^2} + \frac{1}{x\sin\theta_c + y\cos\theta_c}\left(\frac{\partial p}{\partial x}\sin\theta_c + \frac{\partial p}{\partial y}\cos\theta_c\right) + \frac{1}{(x\sin\theta_c + y\cos\theta_c)^2}\frac{\partial^2 p}{\partial \phi^2}.
\end{aligned} \tag{5}$$

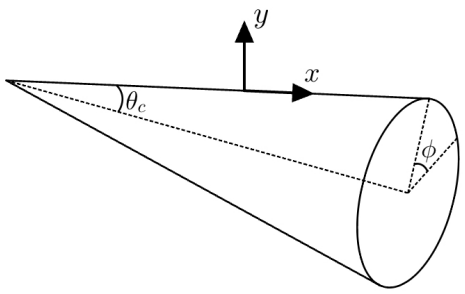

Figure 3: Sketch of the cone, showing the chosen coordinate system

In our coordinate system there are also the relations:

$$\frac{\partial \hat{x}}{\partial \phi} = \sin\theta_c \hat{\phi}\ , \quad \frac{\partial \hat{y}}{\partial \phi} = \cos\theta_c \hat{\phi}\ , \quad \frac{\partial \hat{\phi}}{\partial \phi} = -\left(\sin\theta_c \hat{x} + \cos\theta_c \hat{y}\right). \tag{6}$$

Using the above assumptions and the relations in the coordinate system, Eqs. (1) to (3) become the following:

Continuity:

$$\frac{\partial}{\partial x}(\rho u) + \frac{\partial}{\partial y}(\rho v) + \rho \frac{u\sin\theta_c + v\cos\theta_c}{x\sin\theta_c + y\cos\theta_c} = 0, \tag{7}$$

$\hat{x}$**–momentum:**

$$\begin{aligned}
&\rho\left(u\frac{\partial u}{\partial x} + v\frac{\partial u}{\partial y} - \frac{w^2\sin\theta_c}{x\sin\theta_c + y\cos\theta_c}\right) + R\frac{\partial}{\partial x}(\rho T) = \\
&= \mu\left[\frac{4}{3}\frac{\partial^2 u}{\partial x^2} + \frac{\partial^2 u}{\partial y^2} + \frac{1}{3}\frac{\partial^2 v}{\partial x \partial y} + \frac{1}{x\sin\theta_c + y\cos\theta_c}\left(\frac{4}{3}\frac{\partial u}{\partial x}\sin\theta_c + \frac{\partial u}{\partial y}\cos\theta_c + \frac{1}{3}\frac{\partial v}{\partial x}\cos\theta_c\right) - \right. \\
&\left. - \frac{4}{3}\frac{u\sin^2\theta_c + v\sin\theta_c\cos\theta_c}{(x\sin\theta_c + y\cos\theta_c)^2}\right] + \frac{\partial \mu}{\partial x}\left(\frac{4}{3}\frac{\partial u}{\partial x} - \frac{2}{3}\frac{\partial v}{\partial y} - \frac{2}{3}\frac{u\sin\theta_c + v\cos\theta_c}{x\sin\theta_c + y\cos\theta_c}\right) + \frac{\partial \mu}{\partial y}\left(\frac{\partial u}{\partial y} + \frac{\partial v}{\partial x}\right),
\end{aligned} \tag{8}$$

$\hat{y}$**–momentum:**

$$\begin{aligned}
&\rho\left(u\frac{\partial v}{\partial x} + v\frac{\partial v}{\partial y} - \frac{w^2\cos\theta_c}{x\sin\theta_c + y\cos\theta_c}\right) + R\frac{\partial}{\partial y}(\rho T) = \\
&= \mu\left[\frac{1}{3}\frac{\partial^2 u}{\partial x \partial y} + \frac{\partial^2 v}{\partial x^2} + \frac{4}{3}\frac{\partial^2 v}{\partial y^2} + \frac{1}{x\sin\theta_c + y\cos\theta_c}\left(\frac{1}{3}\frac{\partial u}{\partial y}\sin\theta_c + \frac{\partial v}{\partial x}\sin\theta_c + \frac{4}{3}\frac{\partial v}{\partial y}\cos\theta_c\right) - \right. \\
&\left. - \frac{4}{3}\frac{u\sin\theta_c\cos\theta_c + v\cos^2\theta_c}{(x\sin\theta_c + y\cos\theta_c)^2}\right] + \frac{\partial \mu}{\partial x}\left(\frac{\partial u}{\partial y} + \frac{\partial v}{\partial x}\right) + \frac{\partial \mu}{\partial y}\left(-\frac{2}{3}\frac{\partial u}{\partial x} + \frac{4}{3}\frac{\partial v}{\partial y} - \frac{2}{3}\frac{u\sin\theta_c + v\cos\theta_c}{x\sin\theta_c + y\cos\theta_c}\right),
\end{aligned} \tag{9}$$

$\hat{\phi}$**–momentum:**

$$\begin{aligned}
&\rho\left(u\frac{\partial w}{\partial x} + v\frac{\partial w}{\partial y} + w\frac{u\sin\theta_c + v\cos\theta_c}{x\sin\theta_c + y\cos\theta_c}\right) = \\
&= \mu\left[\frac{\partial^2 w}{\partial x^2} + \frac{\partial^2 w}{\partial y^2} + \frac{1}{x\sin\theta_c + y\cos\theta_c}\left(\frac{\partial w}{\partial x}\sin\theta_c + \frac{\partial w}{\partial y}\cos\theta_c\right) - \frac{w}{(x\sin\theta_c + y\cos\theta_c)^2}\right] + \\
&+ \frac{\partial \mu}{\partial x}\left(\frac{\partial w}{\partial x} - \frac{w\sin\theta_c}{x\sin\theta_c + y\cos\theta_c}\right) + \frac{\partial \mu}{\partial y}\left(\frac{\partial w}{\partial y} - \frac{w\cos\theta_c}{x\sin\theta_c + y\cos\theta_c}\right),
\end{aligned} \tag{10}$$

Energy:

$$\rho C_p\left(u\frac{\partial T}{\partial x}+v\frac{\partial T}{\partial y}\right)=R\left(u\frac{\partial}{\partial x}\left(\rho T\right)+v\frac{\partial}{\partial y}\left(\rho T\right)\right)+$$
$$+\frac{C_p}{Pr}\left\{\mu\left[\frac{\partial^2 T}{\partial x^2}+\frac{\partial^2 T}{\partial y^2}+\frac{1}{x\sin\theta_c+y\cos\theta_c}\left(\frac{\partial T}{\partial x}\sin\theta_c+\frac{\partial T}{\partial y}\cos\theta_c\right)\right]+\frac{\partial\mu}{\partial x}\frac{\partial T}{\partial x}+\frac{\partial\mu}{\partial y}\frac{\partial T}{\partial y}\right\}+$$
$$+\mu\left\{\frac{4}{3}\left[\left(\frac{\partial u}{\partial x}\right)^2+\left(\frac{\partial v}{\partial y}\right)^2-\frac{\partial u}{\partial x}\frac{\partial v}{\partial y}+\left(\frac{u\sin\theta_c+v\cos\theta_c}{x\sin\theta_c+y\cos\theta_c}\right)^2-\left(\frac{\partial u}{\partial x}+\frac{\partial v}{\partial y}\right)\frac{u\sin\theta_c+v\cos\theta_c}{x\sin\theta_c+y\cos\theta_c}\right]+\right.$$
$$\left.+\left(\frac{\partial u}{\partial y}+\frac{\partial v}{\partial x}\right)^2+\left(\frac{\partial w}{\partial x}-\frac{w\sin\theta_c}{x\sin\theta_c+y\cos\theta_c}\right)^2+\left(\frac{\partial w}{\partial y}-\frac{w\cos\theta_c}{x\sin\theta_c+y\cos\theta_c}\right)^2\right\}. \tag{11}$$

3.2 Boundary Layer Equations

Using dimensional analysis, appropriate equations for the BL are obtained. Let us introduce some dimensionless variables:

$$u=u_e\tilde{u}\ ,\ v=V\tilde{v}\ ,\ w=W\tilde{w}\ ,\ \rho=\rho_e\tilde{\rho}\ ,\ T=T_e\tilde{T}\ ,\ \mu=\mu_e\tilde{\mu}\ ,\ x=L\tilde{x}\ ,\ y=\delta\tilde{y}. \tag{12}$$

Since the BL is thin, i.e. $L\gg\delta$, we can neglect some terms based on their order of magnitude. Because we would like to examine realistic cone's semi-angles, we will consider the case of $\tan\theta_c\gg\delta/L$. In addition, the dimensional analysis yields that the normal velocity scales as $V\sim u_e\delta/L$ and the condition $Re_e\sim(L/\delta)^2$, in order to have rotating advection. That is the case we want to consider, to investigate the influence of the rotation. It is important to note that all constants such as γ, Pr and M_e^2 are of $\mathcal{O}(1)$, where M_e is found by solutions of the Taylor-Maccoll flow outside the boundary layer, as explained in Appendix (A). The remaining term to check is the order of $(W/u_e)^2$. Since the flow in $\hat{\phi}$–direction is a secondary flow, it is reasonable to assume that $W/u_e\ll 1$. Using that condition along with $Re_e\sim(L/\delta)^2$ from before, and omitting the $\tilde{(\cdot)}$ from the dimensionless variables, Eqs. (7) to (11) become:

Continuity:

$$\frac{1}{x}\frac{\partial}{\partial x}\left(x\rho u\right)+\frac{\partial}{\partial y}\left(\rho v\right)=0, \tag{13}$$

$\hat{x}$–momentum:

$$\rho\left(u\frac{\partial u}{\partial x}+v\frac{\partial u}{\partial y}\right)=\frac{\partial}{\partial y}\left(\mu\frac{\partial u}{\partial y}\right), \tag{14}$$

$\hat{y}$–momentum & ideal gas:

$$\rho T=\rho_e T_e, \tag{15}$$

$\hat{\phi}$–momentum:

$$\rho\left(\frac{u}{x}\frac{\partial}{\partial x}\left(xw\right)+v\frac{\partial w}{\partial y}\right)=\frac{\partial}{\partial y}\left(\mu\frac{\partial w}{\partial y}\right), \tag{16}$$

Energy:

$$\rho C_p\left(u\frac{\partial T}{\partial x}+v\frac{\partial T}{\partial y}\right)=\frac{C_p}{Pr}\frac{\partial}{\partial y}\left(\mu\frac{\partial T}{\partial y}\right)+\mu\left(\frac{\partial u}{\partial y}\right)^2. \tag{17}$$

These equations can be also obtained by the equations from subsection 12.1.4 – "Boundary Layers on Rotating Bodies of Revolution" in Schlichting & Gersten (2017).

3.3 Boundary Conditions

The above equations are supplemented by appropriate boundary conditions (BC). Since we have a relation between ρ and μ to T, our 4 unknowns are: u, v, w, T. The system of equations has higher derivatives of 2^{nd} order for u, w, T and 1^{st} order for v. Thus, two BC's are required for u, w, T, and one BC for v. On the wall (cone's body) the BC's are impermeability, no-slip and isothermal wall. At the BL edge, the properties have to reach the TM solution values. That yields:

$$\begin{aligned} y = 0: &\qquad u = 0\ ,\ v = 0\ ,\ w = w_w(x)\ ,\ T = T_w, \\ y \to \infty: &\qquad u = u_e\ ,\ w = 0\ ,\ T = T_e, \end{aligned} \tag{18}$$

where the BC for w on the wall is due to angular rotation, $w_w(x) = \Omega x \sin\theta_c$. Another possible boundary condition for the wall temperature is the adiabatic case where at $y = 0$ there is no heat flux, i.e. $\partial T/\partial y = 0$. Hereafter, we continue with the isothermal case.

3.4 Similarity Equations

Self-similarity is a method to reduce a set of partial differential equations (PDE) to a set of ordinary differential equations (ODE). Using the Stewartson-Illingworth transformation (Stewartson, 1949; Illingworth, 1949), the following transformed variables are chosen:

$$\xi = \int_0^x \rho_e u_e \mu_e \,\mathrm{d}x = \rho_e u_e \mu_e x \quad , \quad \eta = \frac{1}{\delta(x)} \int_0^y \frac{\rho}{\rho_e} \,\mathrm{d}y\,, \tag{19}$$

where η is the similarity variable and $\delta(x)$ is the BL thickness. Under the assumption of self-similarity, our variables are expressed as functions of only η,

$$\frac{u}{u_e} = F'(\eta) \quad , \quad \frac{T}{T_e} = \Theta(\eta) \quad , \quad \frac{w}{w_w(x)} = G(\eta), \tag{20}$$

where $(\cdot)' = \mathrm{d}(\cdot)/\mathrm{d}\eta$. The density, ρ, and viscosity, μ, are given by

$$\frac{\rho}{\rho_e} = \frac{1}{\Theta(\eta)} \quad , \quad \frac{\mu}{\mu_e} = \Theta^\sigma(\eta). \tag{21}$$

To transform the equations, partial derivatives of the transformation variables are required,

$$\begin{aligned} \frac{\partial \xi}{\partial x} &= \rho_e u_e \mu_e \quad , \quad \frac{\partial \xi}{\partial y} = 0, \\ \frac{\partial \eta}{\partial x} &= \dots \quad , \quad \frac{\partial \eta}{\partial y} = \frac{1}{\delta(\xi)} \frac{\rho}{\rho_e} = \frac{1}{\delta(\xi)\Theta(\eta)}, \end{aligned} \tag{22}$$

where the BL thickness δ can be expressed in terms of ξ instead of x. The partial derivative $\partial\eta/\partial x$ is not written explicitly since it vanishes during the derivation. Moreover, the derivations yields the following expression for the BL thickness:

$$\delta(\xi) = \frac{1}{\rho_e u_e} \sqrt{\frac{2}{3} \bar{C}_1 \xi}, \tag{23}$$

where $\bar{C}_1$ is a constant. It can be chosen arbitrary, so let us choose $\bar{C}_1 = 3$, such that the BL thickness is the same as for the flat plate case. It reads as:

$$\delta(\xi) = \frac{\sqrt{2\xi}}{\rho_e u_e} \quad \Longrightarrow \quad \delta(x) = \sqrt{\frac{2}{Re_{e,x}}}x, \tag{24}$$

where $Re_{e,x} = \rho_e u_e x/\mu_e$ is the edge Reynolds number based on position x. Thus the BL thickness is consistent with the flat plate case. In addition, using the relations between C_p, C_v and γ, and introducing the Mach number at the BL edge, $M_e = u_e/\sqrt{\gamma R T_e}$, the similarity form of Eqs. (13) to (17) becomes:

$\hat{x}$–**momentum:**

$$3FF'' + (\sigma - 1)\Theta^{\sigma-2}\Theta' F'' + \Theta^{\sigma-1}F''' = 0, \tag{25}$$

$\hat{\phi}$–**momentum:**

$$3FG' + (\sigma - 1)\Theta^{\sigma-2}\Theta' G' + \Theta^{\sigma-1}G'' - 4F'G = 0, \tag{26}$$

Energy:

$$3PrF\Theta' + (\sigma - 1)\Theta^{\sigma-2}\left(\Theta'\right)^2 + \Theta^{\sigma-1}\Theta'' + (\gamma - 1)PrM_e^2\left(F''\right)^2\Theta^{\sigma-1} = 0. \tag{27}$$

The above expression for the BL thickness, Eq. (24), yields the non-dimensional wall-normal coordinate, which is:

$$\frac{y}{\delta(x)} = \int_0^\eta \Theta(\bar{\eta})\,\mathrm{d}\bar{\eta}\,, \tag{28}$$

where the integral can be evaluated, e.g. using the "trapezoidal rule".

3.5 Numerical Method

The similarity equations we obtained, Eqs. (25) to (27), are a nonlinear coupled set of ODE's for $F(\eta), \Theta(\eta)$ and $G(\eta)$. Thus, a numerical solution is required. Let us define the following state vector:

$$\vec{X} = [X_1, X_2, X_3, X_4, X_5, X_6, X_7] = \left[F(\eta), F'(\eta), F''(\eta), \Theta(\eta), \Theta'(\eta), G(\eta), G'(\eta)\right]. \tag{29}$$

Substituting $\vec{X}$ into the similarity equations, and rearranging, we get:

$$\begin{aligned}
&X_1' = X_2, \qquad X_2' = X_3, \qquad X_3' = (1-\sigma)X_3X_4^{-1}X_5 - 3X_1X_3X_4^{1-\sigma},\\
&X_4' = X_5, \qquad X_5' = (1-\sigma)X_4^{-1}X_5^2 - 3PrX_1X_4^{1-\sigma}X_5 - (\gamma-1)PrM_e^2X_3^2,\\
&X_6' = X_7, \qquad X_7' = 4X_2X_4^{1-\sigma}X_6 - 3X_1X_4^{1-\sigma}X_7 + (1-\sigma)X_4^{-1}X_5X_7.
\end{aligned} \tag{30}$$

As can be seen, X_6 and X_7 are decoupled of the other state variables. Thus, we can solve for X_1, X_2, X_3, X_4, X_5 first and then use them to solve for X_6, X_7. The set of equations in Eq. (30) is subjected to the following boundary conditions:

$$\begin{aligned}
&\eta = 0: \qquad X_1 = 0\ ,\ X_2 = 0\ ,\ X_4 = \Theta_w\ ,\ X_6 = 1,\\
&\eta \to \infty: \qquad X_2 = 1\ ,\ X_4 = 1\ ,\ X_6 = 0,
\end{aligned} \tag{31}$$

where the dimensionless wall temperature is $\Theta_w = T_w/T_e$.

We would like to solve the set of equations in Eq. (30) by using methods of initial-value problems (IVP), such as Runge-Kutta. Therefore, we need to guess another 3 'initial conditions' for X_3, X_5, X_7 at $\eta = 0$. This is called the 'Shooting Method', where we guess extra 'initial conditions' and check if the unused BC are satisfied.

3.6 Solution Procedure

The solution procedure is illustrated in the flow chart shown in Fig. (4).

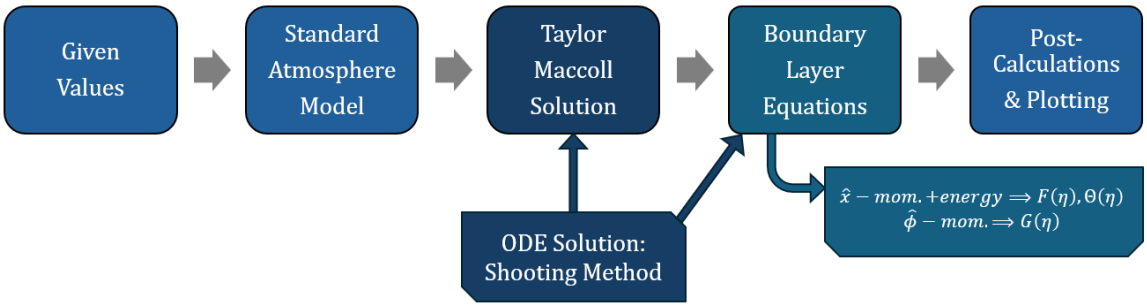

Figure 4: Solution procedure flow chart

4 Results

The solution of the similarity equations, Eqs. (25) to (27), is obtained using the numerical procedure explained above. Let us examine a $L = 1\,[m]$ length cone with half-angle $\theta_c = 10°$, flying at an altitude of $h = 20\,[km]$ and velocity of $U_\infty = 1000\,[m/sec]$. According to the Standard Atmosphere model these flight conditions yield a Mach number of $M_\infty = 3.4$, and the following ambient conditions:

$$p_\infty = 5.5\,[kPa] \quad , \quad \rho_\infty = 0.088\left[\frac{kg}{m^3}\right] \quad , \quad T_\infty = 216.5\,[K] \quad , \quad \mu_\infty = 1.42 \cdot 10^{-5}\left[\frac{kg}{m \cdot sec}\right]. \tag{32}$$

Using the Taylor-Maccoll solution (Taylor & Maccoll, 1933), assuming air is a calorically perfect gas with $\gamma = 1.4,\ R = 287\,[J/(kg \cdot K)]$, we get the following BL edge conditions:

$$\begin{aligned} M_e = 3.04 \quad , \quad p_e = 9.13\,[kPa] \quad , \quad \rho_e = 0.127\left[\frac{kg}{m^3}\right], \\ T_e = 251\,[K] \quad , \quad \mu_e = 1.59 \cdot 10^{-5}\left[\frac{kg}{m \cdot sec}\right] \quad , \quad u_e = 964.7\left[\frac{m}{sec}\right]. \end{aligned} \tag{33}$$

In addition, we consider the isothermal case with a wall temperature of $T_w = 300\,[K]$, which yields the dimensionless wall temperature $\Theta_w \approx 1.2$, and assuming air with $Pr = 0.7,\ \sigma = 0.75$.

The solution of the similarity equations is normalized by the appropriate scaling factor to make sure that the BL edge will be at $y/\delta(x) = 1$. Since $F''(\eta) \to 0$ at the BL edge, we will define it by taking $F''(\eta) = 0.01$. That yields a scaling factor of ≈ 3.93 for $\theta_c = 10°$.

4.1 Main Results

The solution profiles for the dimensionless streamwise and azimuthal velocity components and temperature are shown in Figs. (5) to (7). Note that in terms of the similarity functions:

$$\frac{u}{u_e} = F'(\eta) \quad , \quad \frac{T}{T_e} = \Theta(\eta) \quad , \quad \frac{w}{w_w(x)} = G(\eta). \tag{34}$$

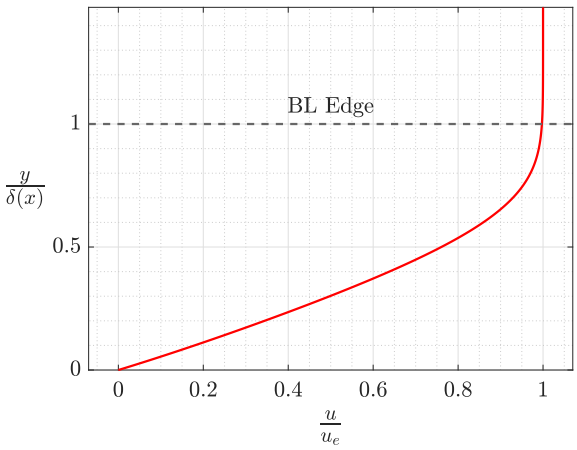

Figure 5: Streamwise velocity profile

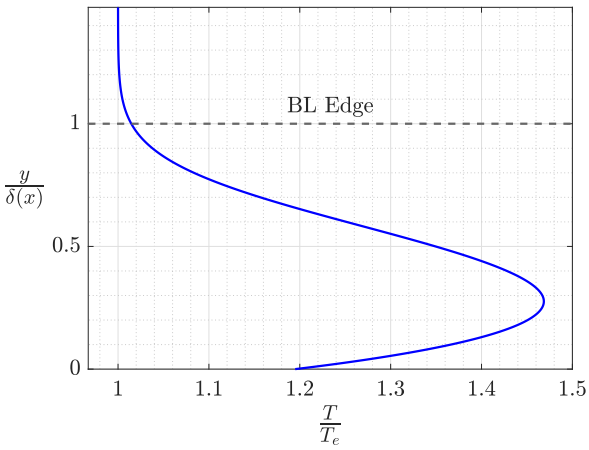

Figure 6: Temperature profile

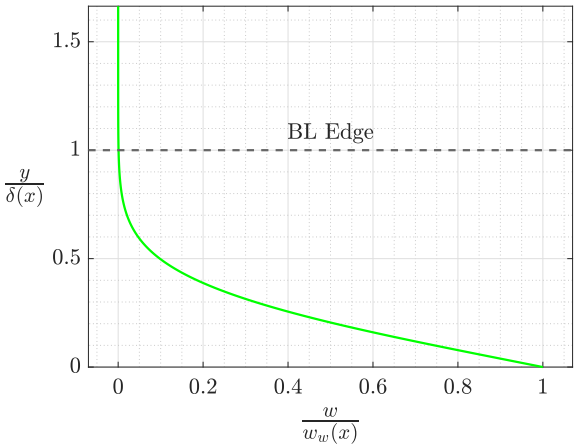

Figure 7: Azimuthal velocity profile

As can be seen above, the results match our theoretical expectations. The BC are satisfied – the streamwise velocity and temperature both approach 1 at infinity, while the azimuthal velocity approaches 0. At the wall the streamwise velocity is 0, the azimuthal velocity is 1 and the temperature approaches Θ_w. In addition, the temperature reaches a maximum inside the BL. This phenomenon, referred to as a "cold wall", occurs when $T_w < T_{0e}$, where T_{0e} is the BL edge stagnation temperature, which depends only on M_e.

4.2 Additional Results

Using the above results, other interesting quantities of the BL can be calculated. Since a compressible BL is considered, it is useful to calculate the Mach number, whose profile is shown if Fig. (8). In terms of the similarity functions:

$$M = \frac{|\vec{u}|}{a} \approx \frac{u}{\sqrt{\gamma RT}} = \frac{u_e F'}{\sqrt{\gamma R T_e \Theta}} = M_e \frac{F'}{\sqrt{\Theta}}. \tag{35}$$

Furthermore, let us calculate the stagnation temperature in the BL. Its profile is shown in Fig. (9). In terms of the similarity functions:

$$\frac{T_0}{T_{0e}} = \frac{T_e}{T_{0e}} \frac{T_0}{T_e} = \frac{T_e}{T_{0e}} \frac{\left(T + \frac{u^2}{2C_p}\right)}{T_e} = \frac{T_e}{T_{0e}} \left(\frac{T}{T_e} + \frac{u_e^2 \left(F'\right)^2}{2C_p T_e}\right) = \frac{T_e}{T_{0e}} \left(\Theta + \frac{\gamma - 1}{2} M_e^2 \left(F'\right)^2\right). \tag{36}$$

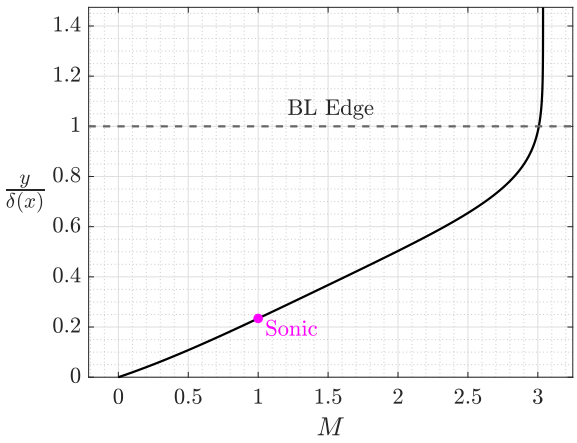

Figure 8: Mach number profile

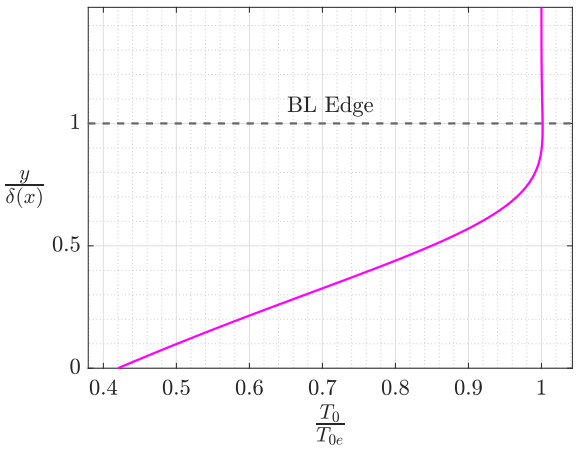

Figure 9: Stagnation temperature profile

In Fig. (8), a region of subsonic flow is observed, located roughly at the bottom quarter of the BL. In Fig. (9), a monotonic decrease of the stagnation temperature towards the body is attained. That is attributed to our examination of an isothermal case with $Pr \neq 1$. This is in contrast to the adiabatic case with $Pr = 1$, where the stagnation temperature remains uniform throughout the BL.

4.3 Streamlines & Reynolds Number

Furthermore, we would like to examine the streamlines in the BL. The function $\mathcal{H}(x, y)$ is defined to be constant on the streamlines – the lines that the planar velocity vector, $\vec{u} = u\hat{x} + v\hat{y}$, is tangent to, while considering the density variation across the BL. That yields:

$$\rho\vec{u} \cdot \vec{\nabla}\mathcal{H} = 0 \quad \Longrightarrow \quad \frac{\partial \mathcal{H}}{\partial y} = \rho u \ , \ \frac{\partial \mathcal{H}}{\partial x} = -\rho v. \tag{37}$$

Note that the relations in Eq. (37) do not satisfy the continuity equation, which is different from the standard "streamfunction" definition. Using the obtained similarity solution, the expressions for the function $\mathcal{H}(x, y)$ and the velocity components $u(x, y)$ and $v(x, y)$ can be written as:

$$\begin{aligned} u(x,y) &= u\big(\xi(x,y), \eta(x,y)\big) = u_e F'(\eta), \\ v(x,y) &= v\big(\xi(x,y), \eta(x,y)\big) = \rho_e u_e^2 \mu_e \frac{\mathrm{d}\delta(\xi)}{\mathrm{d}\xi} \left(F'(\eta) \int_0^\eta \Theta(\bar{\eta})\, \mathrm{d}\bar{\eta} - F(\eta)\Theta(\eta) \right), \\ \mathcal{H}(x,y) &= \mathcal{H}\big(\xi(x,y), \eta(x,y)\big) = \rho_e u_e \delta(\xi) F(\eta). \end{aligned} \tag{38}$$

The normalized velocity components, $u(x, y)/u_e$ and $v(x, y)/u_e$, are shown in Figs. (10) and (11), respectively. As can be seen, the streamwise velocity component approaches 1 outside of the BL edge, $\delta(x)$, as it satisfies the similarity solution. The normal velocity component is positive in the whole field, which indicates of a outbound mass flux at the BL edge. This phenomenon can also be seen in Fig. (12), where the streamlines shift away from the wall. Moreover, it is noticeable that the normal velocity is at least an order of magnitude less than the streamwise velocity, in accordance with the BL assumption that $v \ll u$.

Additionally, because we consider a viscous flow, it can be interesting to calculate the local

Reynolds number which is shown in Fig. (13). In terms of the similarity functions:

$$Re_x = \frac{\rho u x}{\mu} = \frac{\xi}{\mu_e^2} \frac{F'(\eta)}{\Theta^{\sigma+1}(\eta)}. \tag{39}$$

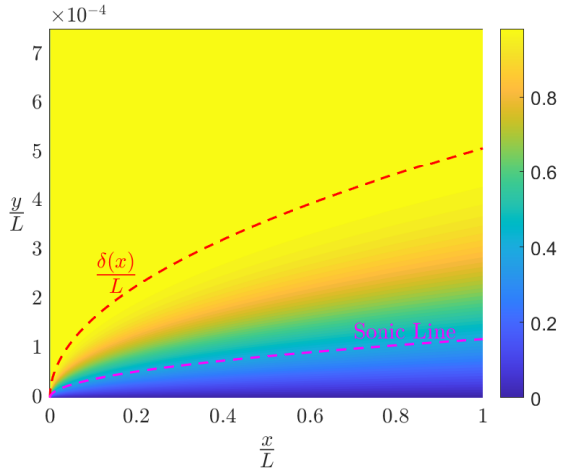

Figure 10: Streamwise velocity, u/u_e

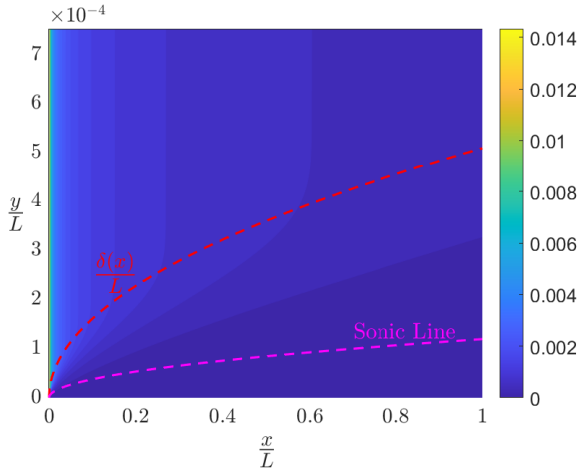

Figure 11: Normal velocity, v/u_e

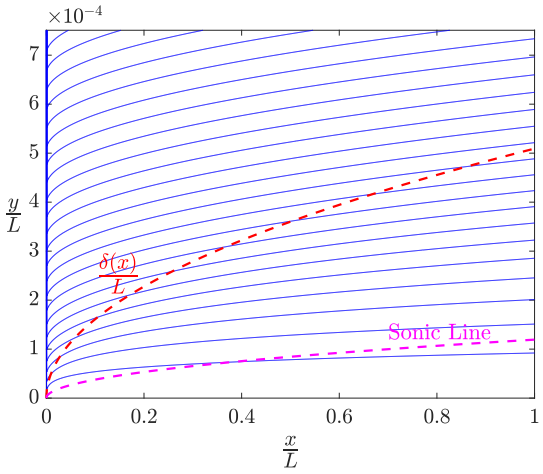

Figure 12: Streamlines, $\mathcal{H}/(\rho_e u_e L)$

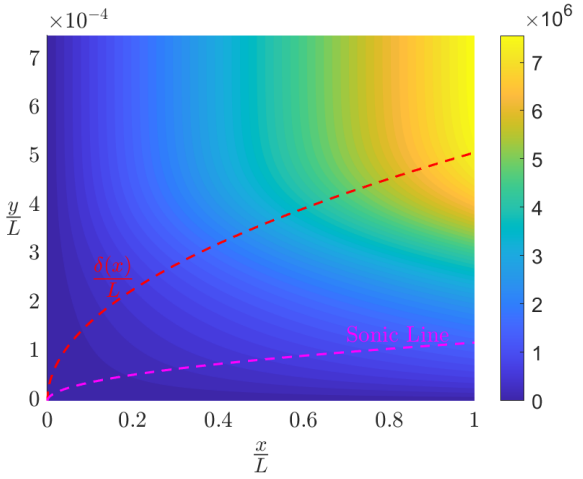

Figure 13: Local Reynolds number, Re_x

4.4 Effect of the Cone's Half-Angle

A key parameter in the problem is the cone's half-angle θ_c. Let us consider a cone at the same flight conditions as in Section (4.1), yielding $M_\infty = 3.4$. The other parameters, γ, R, T_w, Pr, σ, remain the same as before. Let us compare between various cone half-angles, $\theta_c = 10°, 20°, 30°, 40°, 50°$, for each of whom the BL edge Mach number, M_e, changes. It is important to note that at this specific M_∞, the shock remains attached to the cone's tip for all of these angles, otherwise our analysis is invalid. The results are shown in Fig. (14).

It can be inferred from Fig. (14) that there are differences in the temperature profiles for various θ_c, while the variation in the velocity profiles is not as significant. In Fig. (14a) and Fig. (14b), we see that the streamwise and azimuthal velocities change slightly with θ_c. The Mach number, Fig. (14e), varies since it is not normalized by M_e, which shows that for high cone's half-angles the BL edge becomes subsonic. In Fig. (14c) we can see that as θ_c increases the temperature decreases, even up to cases where there is no maximum. That is attributed to the decrease of M_e with θ_c, which is

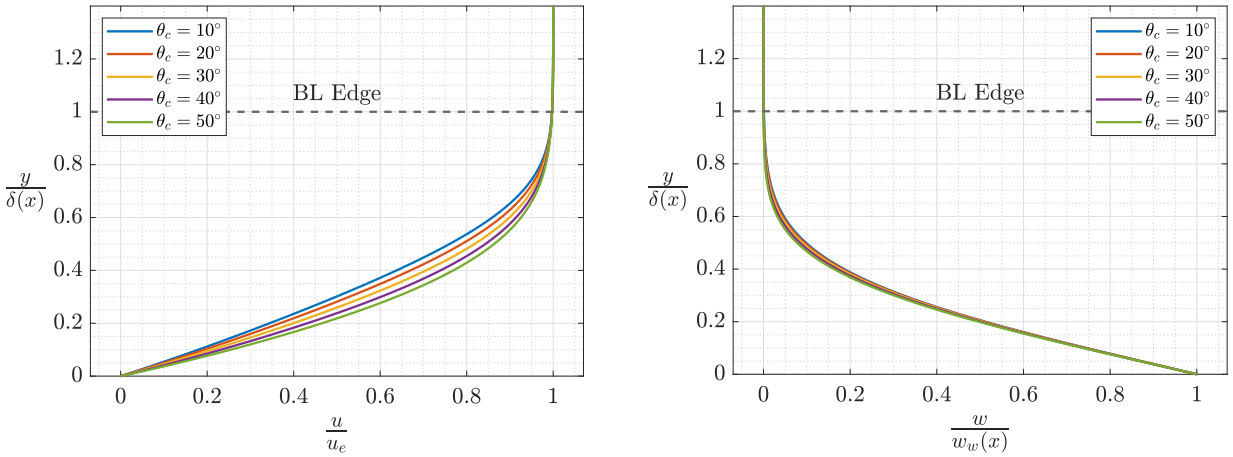

(a) Streamwise velocity

(b) Azimuthal velocity

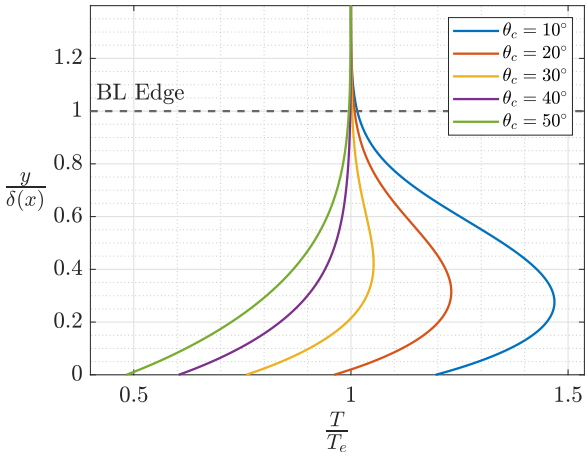

(c) Temperature

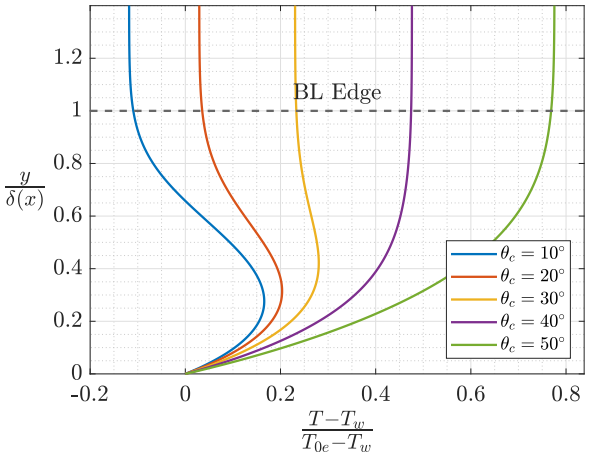

(d) Modified temperature

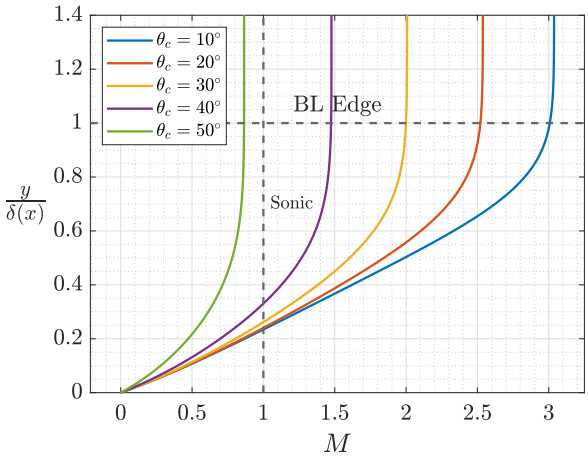

(e) Mach number

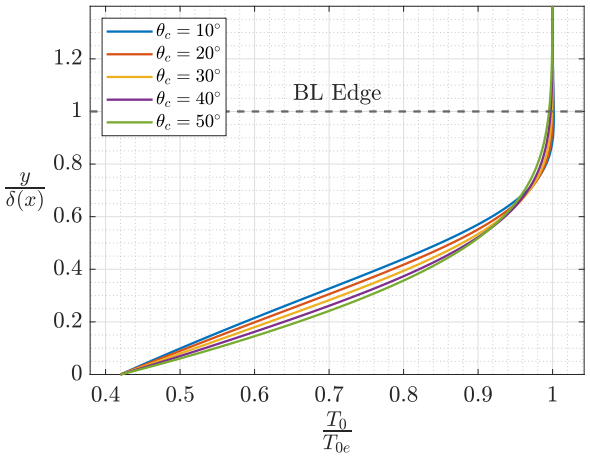

(f) Stagnation temperature

Figure 14: Comparison of different quantities for various cone's half-angles

equivalent to an increase in T_e. Fig. (14d) shows another normalization of the temperature which takes into consideration also the wall temperature, T_w, instead of only the BL edge temperature, T_e or T_{0e}. The "cold wall" phenomenon is seen in Fig. (14d) too for the small θ_c cases. Moreover, as seen in Fig. (14f), the variation of the stagnation temperature, T_0, with θ_c is not as large, similarly to the velocity profiles.

5 Summary & Conclusions

This study examines the flow field in the boundary layer on a rotating cone in supersonic flow. An accurate description of the flow field was attained by deriving the boundary layer equations from the Navier-Stokes equations and transforming them into a self-similar form using the Stewartson-Illingworth transformation (Stewartson, 1949; Illingworth, 1949). A crucial assumption was made regarding the rotation speed being small relative to the streamwise velocity, facilitating the decoupling of the azimuthal momentum equation. The similarity equations were then solved using various ODE solution methods such as "shooting" and Runge-Kutta.

The results obtained from the analysis aligned well with theoretical expectations and highlighted significant physical phenomena within the flow field, including temperature maxima and transitions between subsonic and supersonic flows within the boundary layer.

To further enhance the understanding and accuracy of the results, future investigations are proposed. One approach involves solving the boundary layer equations in spherical coordinates, which can better match the outer flow solutions described by the Taylor-Maccoll solution (Taylor & Maccoll, 1933). Another suggested method is the use of the Mangler transformation (Mangler, 1948), which converts axisymmetric boundary layer equations into flat plate boundary layer equations, potentially eliminating the need for certain limiting assumptions, such as the small rotation assumption, that were made in this study. Finally, exploring the boundary layer flow field using vorticity, a fundamental quantity in boundary layer theory, could provide valuable insights.

In essence, this research contributes to understanding boundary layer dynamics on rotating cones in supersonic flow, offering insights applicable to various engineering domains. By embracing advanced computational techniques and alternative coordinate systems, the study anticipates overcoming current limitations and paving the way for more sophisticated analyses and practical applications in aerodynamics, aerospace engineering, and beyond.

A Order of magnitude of boundary layer edge Mach number

In the dimensional analysis conducted during the derivation of the BL equations, there is a term of the order of M_e^2. We would like to show that this term is not a negligible or dominant term relative to other terms. Using the TM solution (Taylor & Maccoll, 1933), the BL edge Mach number, M_e, was calculated for flight Mach numbers, M_∞, up to 500. The calculations were performed for various cone's half-angles, and the results are presented in Fig. (15).

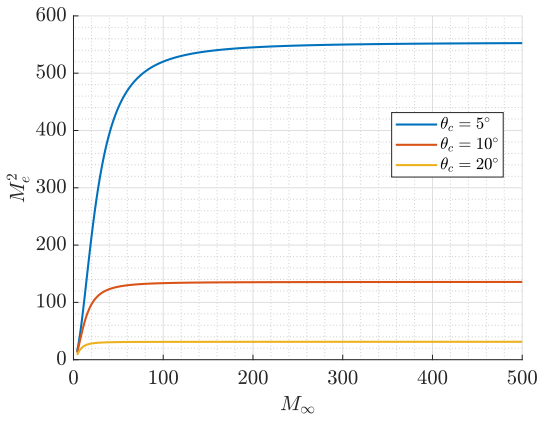

Figure 15: Square of the BL edge Mach number, M_e^2, vs. freestream Mach number, M_∞, for various cone half-angles

As can be seen, M_e^2 has a rapid initial growth, which quickly flattens towards a limit. This is a demonstration of the well-known "Mach Independence" principle by Oswatitsch (1951). As the cone's half-angle increases, M_e^2 decreases. However, as θ_c approaches small angles, M_e^2 grows to a large (finite) value. That is attributed to the fact that when $\theta_c \to 0$, the shock eventually becomes a Mach wave and $M_e \to M_\infty$.

Nevertheless, for realistic values of θ_c, the value of M_e^2 remains finite and not too big to consider it as the dominant order. Thus, this term of the order of M_e^2 should remain in the BL equations and not overtake the other terms.

References

Blasius, H. 1908 Grenzschichten in flüssigkeiten mit kleiner reibung. *Z. Math. Physik* **56**, 1–37, english translation in NACA-TM-1256.

Cohen, C.B. & Reshotko, E. 1956 Similar solutions for the compressible laminar boundary layer with heat transfer and pressure gradient. *Tech. Rep.*. NACA-TN-3325.

Crocco, L. 1937 Eine neue stromfunktion für die erforschung der bewegung der gase mit rotation. *ZAMM - Journal of Applied Mathematics and Mechanics / Zeitschrift für Angewandte Mathematik und Mechanik* **17** (1), 1–7.

Falkner, V.M. & Skan, S.W. 1931 Solutions of the boundary-layer equations. *The London, Edinburgh, and Dublin Philosophical Magazine and Journal of Science* **12** (80), 865–896.

Geis, T., Görtler, H. & Tollmien, W. 1955 *Ähnliche Grenzschichten an Rotationskörpern*, pp. 294–303. Wiesbaden: Vieweg+Teubner Verlag.

Illingworth, C.R. 1949 Steady flow in the laminar boundary layer of a gas. *Proceedings of the Royal Society of London. Series A. Mathematical and Physical Sciences* **199** (1059), 533–558.

Illingworth, C.R. 1953 The laminar boundary layer of a rotating body of revolution. *The London, Edinburgh, and Dublin Philosophical Magazine and Journal of Science* **44** (351), 389–403.

Mangler, W. 1948 Zusammenhang zwischen ebenen und rotationssymmetrischen grenzschichten in kompressiblen flüssigkeiten. *ZAMM - Journal of Applied Mathematics and Mechanics / Zeitschrift für Angewandte Mathematik und Mechanik* **28** (4), 97–103.

Oswatitsch, K. 1951 Ähnlichkeitsgesetz für hyperschallströmung. *ZAMP* **II**, 249–264, Similarity Laws for Hypersonic Flow. Royal Institute of Technology. Stockholm, Sweden. KTH-AERO TN 16 (1950).

Pokrovskii, A. N., Shmanenkov, V. N. & Shchuchinov, V. M. 1984 Determination of the parameters of the boundary layer on rotating axisymmetric cones. *Fluid Dynamics* **19** (3), 367–372.

Schlichting, H. & Gersten, K. 2017 *Axisymmetric and Three–Dimensional Boundary Layers*, pp. 321–347. Berlin, Heidelberg: Springer Berlin Heidelberg.

Sedney, R. 1957 Laminar boundary layer on a spinning cone at small angles of attack in a supersonic flow. *J. Aero. Sci.* **24**, 430–436, 455.

Stewartson, K. 1949 Correlated incompressible and compressible boundary layers. *Proceedings of the Royal Society of London. Series A. Mathematical and Physical Sciences* **200** (1060), 84–100.

Taylor, G.I. & Maccoll, J.W. 1933 The air pressure on a cone moving at high speeds. *Proceedings of the Royal Society of London. Series A, Containing Papers of a Mathematical and Physical Character* **139** (838), 278–297.